frontiers | Frontiers in Marine Science

TYPE Original Research
PUBLISHED 24 November 2022
DOI 10.3389/fmars.2022.1038644

OPEN ACCESS

EDITED BY
Keisuke Shimizu,
The University of Tokyo, Japan

REVIEWED BY
Eva Martins,
Escola Superior de Biotecnologia,
Universidade Católica Portuguesa,
Portugal
Shiguo Li,
Research Center for Eco-environmental Sciences (CAS), China

*CORRESPONDENCE
Rongqing Zhang
rqzhang@mail.tsinghua.edu.cn

SPECIALTY SECTION
This article was submitted to Marine Biology, a section of the journal Frontiers in Marine Science

RECEIVED 07 September 2022
ACCEPTED 11 November 2022
PUBLISHED 24 November 2022

CITATION
Wang Y, Zhang R and Liu C (2022) A novel protein CtCBP-1 functions as a crucial macromolecule during mineralization of limpet teeth. *Front. Mar. Sci.* 9:1038644. doi: 10.3389/fmars.2022.1038644

A novel protein CtCBP-1 functions as a crucial macromolecule during mineralization of limpet teeth

Yadong Wang[1], Rongqing Zhang[2,3,4]* and Chuang Liu[5]

[1]School of Light Industry, Beijing Technology and Business University, Beijing, China, [2]Ministry of Education Key Laboratory of Protein Sciences, School of Life Sciences, Tsinghua University, Beijing, China, [3]Zhejiang Provincial Key Laboratory of Applied Enzymology, Yangtze Delta Region Institute of Tsinghua University, Jiaxing, China, [4]College of Biological, Chemical Sciences and Engineering, Jiaxing University, Jiaxing, China, [5]College of Oceanography, Hohai University, Nanjing, Jiangsu, China

Limpets are a class of marine mollusks that use mineralized teeth, one of the hardest and strongest biological materials, to feed on algae on rocks. By combining proteomics and RNA-seq analysis of limpet radula, we identified a novel chitin-binding protein (CtCBP-1) that may play a regulatory role in radula mineralization of *Cellana toreuma*. In this study, the full-length cDNA of CtCBP-1 gene was cloned for the first time, and the protein was successfully expressed *in vitro*. *In vitro* experiments demonstrated that CtCBP-1 binds well to both goethite and chitin, which are key components of the cusp. We studied the function of CtCBP-1 on goethite crystallization *in vitro*, revealing that it changed the morphology of goethite crystals. We also used fluorescence higher resolution imaging to map the binding of CtCBP-1 in radula and found that the distribution of CtCBP-1 on radula was specific, which consistent with the SEM results finding tightly aligned goethite. In this study, a novel protein CtCBP-1, which regulates the distinctive biomineralization process of limpet teeth, is identified for the first time. This protein's identification may inform biomimetic techniques for creating hard materials that can withstand ambient temperature.

KEYWORDS

limpet teeth, CtCBP-1, crystallization, cellana toreuma, goethite

Introduction

Biomineralization is the process of orderly deposition of inorganic ions in living organisms under the regulation of biomolecules. It is a widespread biological phenomenon found in many forms in a variety of species, from lower prokaryotes such as magnetic bacteria to higher vertebrates such as humans and also other marine

species such as the marine sponges (Lowenstam and Weiner, 1989; Martins et al., 2019). More than 70 biominerals have been discovered, such as calcium mineralization in shells, iron mineralization in limpet teeth, and silicon mineralization in algae (Lowenstam, 1981). The diverse structure and properties of biological minerals are attributed to the orderly regulation of crystal nucleation and growth by organisms.

Calcium mineralization accounts for approximately fifty percent of biomineralization, with calcium carbonate being the most prevalent biogenetic mineral. Additionally, iron mineralization makes up 40% of biomineralization, and iron minerals, primarily in the form of iron oxides and hydroxides, are primarily found in bacteria and mollusks (Weiner and Dove, 2003). Iron oxide biominerals have been found in magnetotactic bacteria and chiton teeth as magnetite (Fe_3O_4) and in limpet teeth as goethite (α-FeOOH). Both chiton and limpet have a radula, which is a tongue-like organ that originates deep within the mollusk's mouth cavity and extends out of the mouth for the last 2-5 mm. Limpet use its teeth, one of the hardest and stiffest biominerals known (Barber et al., 2015), to harvest endolithic algae from rocks. The anterior region of the tooth cusps used for scraping is referred to as the leading edge, and the corresponding posterior region is referred to as the trailing edge (Weaver et al., 2010; Brooker and Shaw, 2012).

The teeth of chitons and limpet have been used as a unique model for the systematic study of iron mineralization processes, not only due to the good mechanical properties of mineralization products (van der Wal et al., 2000; Grunenfelder et al., 2014; Barber et al., 2015), but also due to the different stages of mineral development that can be observed in a single radula structure (Sone et al., 2005; Sone et al., 2007; Ruggeberg et al., 2010). It has been discovered that the cusps of many species of limpet teeth are constructed of a preformed α-chitin matrix filled with goethite(α-FeOOH) and amorphous hydrated silica ($SiO_2{\cdot}nH_2O$) (Grime et al., 1985; Burford et al., 1986; Mann et al., 1986; Wal, 1989; Lu et al., 1995; Sone et al., 2007). Additionally, the chitin matrix is covered with proteins (Liddiard et al., 2004). Especially in the limpet species *Parella vulgata, athletica* and *caerulae*, the α-chitin matrix was found to consist of ordered, closely spaced chitin fibers with only a few nanometers between adjacent fibers (Sone et al., 2007). These incredibly hard minerals in the teeth of limpets demonstrate their utility in scraping rocks for algae. The morphology of goethite have been well studied by microscopy and spectroscopy methods (Mann et al., 1986; Pierre et al., 1986; Sone et al., 2005; Wang et al., 2018). It was found that the tooth base contains microcrystalline(superparamagnetic) and disordered goethite, while the cusp consists of needle-like goethite crystals (Pierre et al., 1986; Wang et al., 2018). These needle goethites are aligned in the direction of the fibers, and the crystals are smaller in the anterior region and larger in the posterior region (Wal, 1989; Wang et al., 2018).

Previous researches have indicated that organic matrices, including proteins and/or polysaccharides, play an essential part in the biomineralization process in many different biominerals, such as controlling crystal nucleation and leading growth with modulating crystal morphology or shape (Baeuerlein, 2006). Many proteins related to biomineralization have been detected in many biominerals, such as eggshells, corals, pearl layers, and magnetosomes (Fang et al., 2012; Ramos-Silva et al., 2013; Marie et al., 2015; Athanasiadou et al., 2018). The proteins discovered in the magnetosomes of bacteria were shown to exercise morphological control over minerals (Amemiya et al., 2007; Tanaka et al., 2011). In addition, studies targeting the shell formation process revealed that matrix proteins serve a critical function in nucleation, polymorphism, morphology and organization of calcium carbonate crystals (Weiner and Dove, 2003). Many organisms typically have excellent command over crystal growth, employing a completely different strategy that normally applied to synthesis. Therefore, the study of biocrystal growth probably offers novel insights to improve the design and control of synthetic crystal growth. The processes behind the production of limpet teeth, which are crucial for the development of biomimetics, have only lately been deciphered using molecular techniques.

In contrast to matrix proteins involved in calcium crystal mineralization, such as shells and corals, proteins that regulate iron oxide biomineralization are still lacking, with the exception of magnetic bacteria (Lin et al., 2005; Faivre and Godec, 2015). The radula transcriptome of the freshwater snail *Tylomelania sarasinorum* contains gene clusters related with vesicular secretion, chitin binding, and iron transfer (Hilgers et al., 2018). A comprehensive examination of the chiton species *Cryptochiton stelleri* revealed the deposition of ferrihydrite on the tooth cusp, which converts into magnetite between only a few rows of teeth (Stegbauer et al., 2021). In a recent study on limpet *Patella vulgata*, researchers analyzed the transcriptome of each developmental stage of the radula, the organ from which limpet teeth originate, in order to identify sequential changes in gene expression associated with chitin and iron processing and quantify iron and chitin metabolic processes in the radula (Rumney et al., 2022). The iron mineralization of the limpet teeth results from the organism's precise regulation of goethite formation through organic macromolecules. However, research on organic macromolecules has been concentrated on ferritin and a few other well-known proteins, iron mineralization-specific proteins have not been investigated. Based on the previously obtained RNA-seq results and mass spectrometry data of limpet *Cellana toreuma*, we focused on novel proteins containing a chitin-binding domain. We selected six chitin-binding proteins with Gly content above 10% or Cys content above 10% and named them CtCBP-1 to CtCBP-6 (Wang et al., 2018).

In this article, we selected the CtCBP-1 protein for more detailed functional studies. The full-length gene was obtained

from *Cellana toreuma* by RACE-PCR and the recombinant protein was expressed *in vitro*. Its role in the goethite crystallization process was verified by *in vitro* experiments, and its location on the radulae was tested by Cy5 labeling experiments. Hence, this study showed that novel protein CtCBP-1 exhibited goethite binding and morphological modifying abilities.

Materials and methods

Limpet sample preparation

Around two hundred limpets *Cellana toreuma*, with shell length 3-4 cm, were collected around July in 2018 from the rocks in the intertidal zone at Zhou Shan beach, Zhejiang Province, China. The radulae were extracted from limpets, placed on petri dishes to maintain a flat shape, and immediately transferred to a -80°C freezer until further use. For the analyses reported here, freshly thawed radulae were thoroughly washed to remove all organic debris: (i) washed in water, (ii) immersed in 5% NaOH for 24h and (iii) again washed in water.

Cloning and analysis of gene CtCBP-1

Total RNA was extracted from radulae tissue with the standard protocol of TRIzol reagent (Life Technology, Thermo, USA) for general cloning of the genes. The quality of RNA was determined by measuring the $OD_{260/280}$, $OD_{260/230}$ and the quantity of RNA was evaluated by OD_{260} with a NanoDrop Lite spectrophotometer (Thermo Scientific, USA). The extracted RNA was used to synthesize single-stranded cDNA for RACE experiments using the SMARTer RACE cDNA Amplification Kit (Clontech, Japan). 3'RACE-F1, F2 and 5'RACE-F1, F2 primers were used with the primers supplied with the 3'- and 5'-RACE kits, respectively. The full-length sequence of CtCBP-1 was confirmed by the primers CtCBP-1-F and CtCBP-1-R. The deduced amino acid sequence was determined bioinformatically using the ExPASy Translate tool and the signal peptide was predicted by SignalP4.1.

Plasmids construction

The coding region of gene CtCBP-1 without signal peptide was amplified by the primers CtCBP-1-pMAL-F and CtCBP-1-pMAL-R (Table 1). In addition, the CtCBP-1-pMAL-R primer contained a His6-tag, and then the amplified fragment was inserted into the pMAL-c5X vector (New England BioLabs Inc., NEB; USA) downstream of the *E. coli* malE gene encoding maltose binding protein (MBP) to promote the expression of the "soluble" fusion protein MBP tagged CtCBP-1. CtCBP-1 was purified for further functional analyses.

Protein expression and purification

Purified recombinant plasmid pMAL-CtCBP-1 was transformed into Escherichia coli strain Transsetta (DE3) (Transgene, China) for expression. The recombinant cell was cultured in LB(Transgene, China) at 37 °C, and add 0.5 mM isopropyl 1thio-β-D-galactopyranoside (IPTG; SIGMA, USA) when the cell density reached 0.6-0.8, then cultured at 16 16°C overnight. Cells were then collected by centrifugation at 8000 g and 4°C for 5 min. The supernatant was removed and the cell pellet was resuspended with lysis buffer (50 mM Tris, 300 mM NaCl, 20 mM imidazole, pH=8.0). The cells were disrupted by ultrasonic homogeniserc. Then cells were disrupted *via* ultrasonic dismembrator (Sonics & Materials Inc., USA) at 30% power with 4 s pulse on and 6 s pulse off repetition cycle on ice. After centrifugation 12000 g for 40 min at 4 Inc., USA) at 30% poweraliquoted into a fresh tube and incubated for 1h at

TABLE 1 Primers used in this study.

function	name	sequence
Primers used for RACE	5'RACE-F1	CCACCATATCCGCCATTGTTGCCTC
	5'RACE-F2	GACGTTGGCTGGGTCACCGCATA
	3'RACE-F1	CATGTTTTGGTGGATTCTAGCCGCGG
	3'RACE-F2	GCGAGTGCCGAGGTGGTAGTCAC
Primers cloning CtCBP-1 to the expression vector pMAL-c5x	CtCBP-1-pMAL-F*	AGGGAAGGATTTCACATATGGGAGGCCTCAGAGCTCCAGAA
	CtCBP-1-pMAL-R*	TAATTACCTGCAGGGAATTCCTAATGATGATGATGATGGTAGTTGTAGTTGTAGTTATTCCTTTTAGG
Primers cloning CtCBP-1 full length	CtCBP-1-F*	ACATGGGGAACTTACAACCAGTCAAAGAGTC
	CtCBP-1-R*	GGTCTCGGTGACATCGTATAAAAACCAGG

*F, forward; R, reverse.

4°C with gentle rocking in the presence of Nickel-NTA agarose slurry (NEB, USA) that had been pre-equilibrated in lysis buffer. The agarose was washed with washing buffer (50 mM Tris, 300 mM NaCl, 40 mM imidazole, pH=8.0). Finally, the protein rCtCBP-1 was eluted using elution buffer (50 mM Tris, 300 mM NaCl, 400 mM imidazole, pH=8.0) then desalted using Hitrap desalting column (GE Healthcare, USA) to a storage buffer (50 mM Tris, 500 mM NaCl, pH=8.0) and stored at 4°C for future experiments. The fractions were analyzed through SDS-PAGE (12% (w/v) acrylamide) followed by staining with Coomassie blue. The purification of MBP was performed according to the instruction of pMAL-c5x (NEB) (GE Healthcare, USA).

Chitin and goethite crystal binding assay

Synthesis of goethite was according to the literature with modifications (Mohapatra et al., 2005). The steps are as follows: Stock solutions containing 1M ferric nitrate (initial pH 0.92 at room temperature) and 10 M sodium hydroxide were prepared using double distilled water. The pH was then adjusted with 10 M sodium hydroxide until a final value of 11.8 was obtained, and the total volume of slurry was increased to 500 mL. The precipitated slurries were aged for 24 hours at 333 K followed by filtration and washing with distilled water until the filtrates were nitrate-free. The prepared products goethite were dried for 24 hours at 373 K. 10 mg goethite (laboratory preparation) or chitin (Biodee, China) was washed and supplemented with 1 mL storage buffer (50 mM Tris, 500 mM NaCl, pH=8.0) respectively. 60 μg rCtCBP-1/MBP were mixed with prepared goethite or chitin respectively, and the mixtures were incubated at 4 °C for 1 h with gentle rolled. After incubation, the pellets were washed with 1 ml Milli-Q deionized water and storage buffer 3 times each and the liquid flowing through was collected to detect the binding abilities of different proteins. Then the washed materials were also collected separately and treated with loading buffer. SDS-PAGE was performed to analyze the binding properties of CtCBP-1 and MBP.

Scanning electron microscope (SEM)

The morphologies of the cleaned three radular were examined by scanning electron microscope (SEM) (FEI Quanta 200, USA) after being sputter-coated with a thin layer of gold nanoparticles.

In vitro crystallization

Synthesis of goethite was according to the literature with modifications (Mohapatra et al., 2005). In the control group, a quantity of 1 M sodium hydroxide was added to 500 μL of 1M ferric nitrate solution until the pH reached 12.0. The precipitated slurries were aged at 60°C for 24 h, then centrifuged at 3000 rpm for 5 min and washed with distilled water until the filtrates were free of nitrate and sulphate. The prepared products were dried at 100°C for 24 h. In the experiment group, proteins CtCBP-1 (35 μg/ml, 70 μg/ml,140 μg/ml) or MBP (35 μg/ml,70 μg/ml,140 μg/ml) were added to the ferric nitrate solution respectively.

Raman spectra

We used Raman spectroscopy to examine samples (negative control, CtCBP-1 (35 μg/ml, 70 μg/ml,140 μg/ml) and MBP (35 μg/ml,70 μg/ml,140 μg/ml)) from *in vitro* crystallization experiments. The Raman spectra were scanned three times for 20 s in the range of 100 to 1400 cm^{-1} using a LabRAM HR Evolution spectrometer (HORIBA JobinYvon, Japan).

X-ray diffraction (XRD)

We used XRD to examine samples (negative control, CtCBP-1 (35 μg/ml, 70 μg/ml,140 μg/ml) and MBP (35 μg/ml,70 μg/ml,140 μg/ml)) from *in vitro* crystallization experiments. XRD (D8 ADVANCE, Bruker, Germany) was applied in the range 10-90 (2 theta degree).

Cy5 labeling and binding of CtCBP-1 in limpet teeth

The recombinant proteins CtCBP-1 and MBP were labeled with Cy5, respectively. The purified recombinant proteins CtCBP-1 and MBP were desalted into labeling buffer (0.1 M phosphate, 500 mM NaCl, pH=8.3) respectively and the concentration was estimated using A280. The dye solution was prepared by dissolving 1 mg Cy5 NHS ester dye (AAT Bioquest, USA) in 100 μL DMSO and then diluting to 0.1 μg/μL with DMSO. The amount (mg) of the dye used was determined by an empirical formula (0.01 × 855 × protein weight (mg)/25,000). 1mg of the protein and the corresponding volume of the dye were uniformly mixed and then reacted in the dark for 30 minutes at room temperature respectively. The labeled proteins were then desalted in an AKTA system(GE, USA) by HiTrap TM Desalting(GE,USA) into storage buffer(20 mM Tris-HCl, 500 mM NaCl, pH = 7.8). Labeled CtCBP-1 and MBP were further used for *in vitro* distribution experiments. 100 μL of 100 μg/ml labeled CtCBP-1 and MBP were further incubated with NaOH-treated radula for 30 minutes in the dark. The teeth were then washed three times with water and a high salt ion concentration buffer to wash away non-specifically bound proteins. And samples were immersed in buffer and then

observed by super-resolution Ti NSIM system (Structured illumination microscopy, Nikon, Japan).

Results

Identification and bioinformatics analyses of CtCBP-1

We previously identified six chitin-binding proteins that may play an important role in tooth mineralization through proteomic studies of limpet teeth. Based on the abundance of expression at the transcriptome level, we selected the most abundant CtCBP-1 protein for more detailed studies. We applied RACE procedures to clone the 5' and 3' flanking sequences to obtain a complete transcript for CtCBP-1 (GeneBankTM accession number ON263363). The CtCBP-1 gene has a full length of 1236 bp (Figure 1A), and the open reading frame encodes 291 amino acids. CtCBP-1 has a theoretical molecular weight of 29.4 kDa and a theoretical isoelectric point of 4.57, which is an acidic protein. Its amino acid content distribution showed that the three amino acids with the highest abundance were Gly (27.15%), Asn (17.18%), Ser (6.87%), and the cysteine content was also high, with a content of 4.47%. Glycine was found to be dominant in the amino acid analysis of mature teeth (Ukmar-Godec et al., 2015), while cysteine was found to be able to directly promote the formation of goethite at room temperature *in vitro* (Cornell and Schneider, 1989).

The BLASTp software was used to align the homologous sequence of the CtCBP-1 protein in the GenBank database. As a result, we only identified a homologous 46.26% protein sequence in limpet *Lottia gigantea*. It suggested that CtCBP-1 may be a protein sequence unique to limpets. The homologous sequences of CtCBP-1 and hypothetical protein LOTGIDRAFT_238408 were mainly located in a conserved functional region and were chitin-binding domains. In addition, there was no functional study of proteins, so the CtCBP-1 protein was a completely new unknown protein.

Using the SignalP 4.1 program (Nielsen, 2017), we found the presence of an N-terminal signal peptide in CtCBP-1, implying that it is a secreted protein. By the SMART software, we found that CtCBP-1 had two chitin-binding domains (Figure 1B). So it was possible that the protein was secreted outside the cell after expression and bound to the chitin framework to exercise functions during mineralization. In addition, through RADAR software, it was found that this protein had a repetitive sequence of about 50 AA long NG at the C-terminus (Figure 1B). These tandem repeats are common features in bio-mineralization proteins (Miyamoto et al., 1996), bioadhesive proteins (Liu et al., 2015) as well as chitin-binding proteins in the beak (YerPeng et al., 2015).

Expression and purification of recombinant protein CtCBP-1 and maltose binding protein MBP

The recombinant CtCBP-1 was expressed with vector pMAL-c5X and sufficiently purified for *in vitro* functional studies (Figure 1C). The molecular mass of CtCBP-1 (81.4 kD) is almost identical to calculated value (CtCBP-1 with His-tag 12 kD plus MBP 40 kD). What's more, mass spectrum was performed to confirm the protein sequence of CtCBP-1. We also expressed and purified MBP as a negative control (Figure 1D) for further functional analyses. In this research, the recombinant protein MBP-CtCBP-1 with a His6-tag on N-terminal, CtCBP-1, was used for further functional analyses.

Binding of CtCBP-1 to goethite and chitin

Since protein attachment may play a key role in regulating crystal characteristics, it is important to perform goethite and chitin-binding assays to explore the affinity and interaction between CtCBP-1 and different crystal polymorphs. CtCBP-1 was incubated with chitin and goethite, respectively, and then eluted with deionized water, 0.5 M NaCl to wash away the nonspecifically absorbent protein before analyzing the sample by SDS-PAGE. We found that in the MBP control group, deionized water and 0.5M NaCl solution can elute MBP from chitin and goethite. However, in the CtCBP-1 experimental group, CtCBP-1 was separated from chitin and goethite only when the strong denaturing agent existed (Figure 1E). The above results demonstrated that CtCBP-1 expressed *in vitro* can effectively bind to chitin and goethite, which provided a basis for possible regulation of crystal growth.

Goethite crystallization in the presence of CtCBP-1 *in vitro*

To verify the role of protein CtCBP-1 in the formation of goethite, *in vitro* crystallization experiment was performed. Protein CtCBP-1 was added into the reaction at final concentrations of 35, 70 and 140 μg/ml, respectively, and established the same final concentration (35, 70 and 140 μg/ml) of MBP protein as a control to rule out of the effect of the tag. Compared to the typical needle-shape goethite crystals in the negative control group (Figure 2A), the crystals in the MBP group showed no obvious morphology alteration (Figures 2C, E, G), which seemed similar to the goethite needles in the leading parts of the limpet teeth (Wang et al., 2018), indicating that MBP tag had no effect on the crystal polymorphs. On the contrary, the crystals in the CtCBP-1

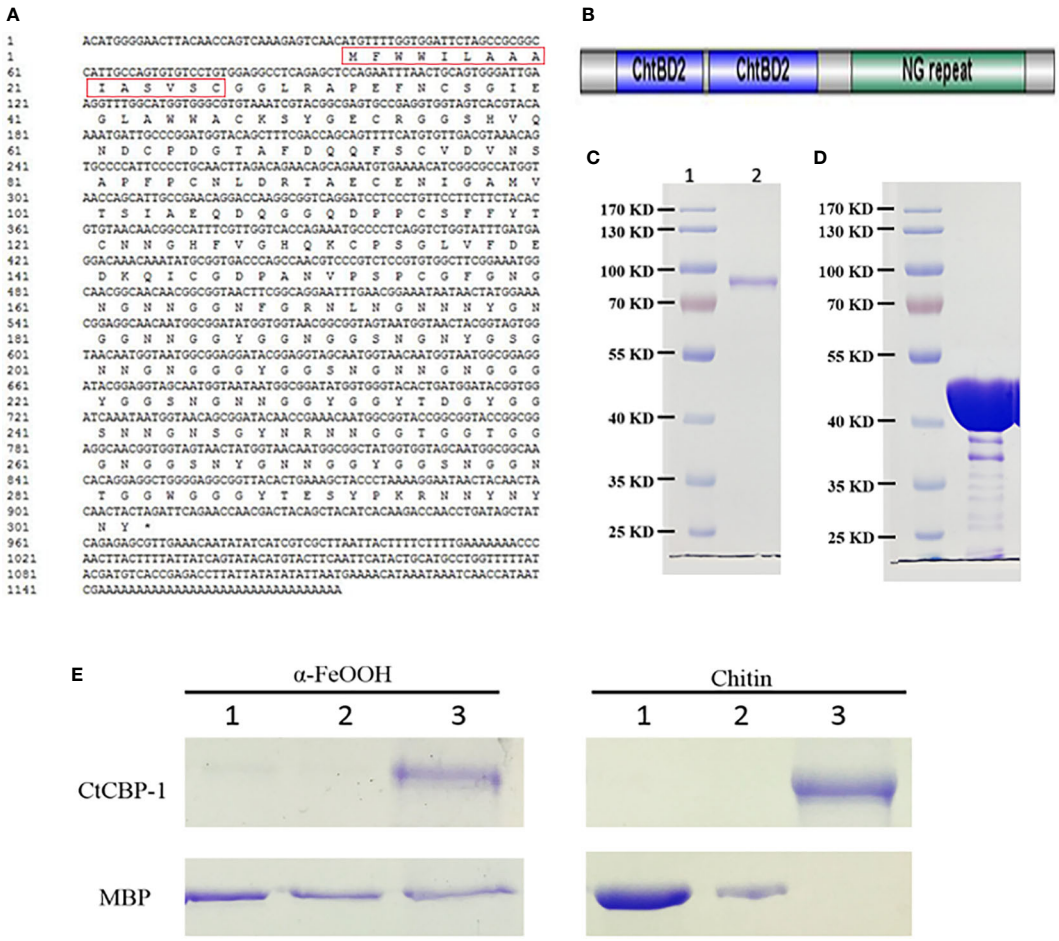

FIGURE 1
(A) The cDNA sequence information of CtCBP-1. Red box is the signal peptide. **(B)** Schematic diagram of the structural domain of CtCBP-1 without signal peptide. **(C)** SDS-PAGE of recombinant protein CtCBP-1 with MBP tag near 80 kD. **(D)** SDS-PAGE of recombinant protein MBP tag at 40 kD. **(E)** Binding properties of CtCBP-1 with goethite and chitin. Lane 1, residual unbound CtCBP-1 and MBP in deionized water wash fraction after incubation with α-FeOOH or chitin; Lane 2, residual unbound CtCBP-1 and MBP in 0.5 M NaCl wash fraction after incubation with α-FeOOH or chitin; Lane 3, the eluate after boiling SDS denaturant containing β-mercaptoethanol for 10 min.

group showed significant changes in crystal morphologies. The morphology of the crystal changes from a typical needle-like goethite morphology to dense precipitates with much smaller crystals and the degree of the morphology alteration increased with elevated concentrations of CtCBP-1 from 35 to 140 μg/mL (Figures 2B, D, F), suggesting that CtCBP-1 affected the crystal morphology. Moreover, it is interesting to note that the altered crystal morphology is similar to the crystal morphology reported in the previous study which was changed by the addition of the chitin framework (Wang et al., 2018). Crystals were analyzed by Raman spectroscopy to confirm the crystal form and indicated that most of the particles in each group were goethite with specific peaks at around 240, 296, 396, 476, 547, and 680 cm-1, indicating that CtCBP-1 and MBP had no effect on the crystal polymorphs (Figure 3).

In the presence of CtCBP-1 protein, the morphology of goethite formed *in vitro* was dissimilar to that of needle-like crystals located at the leading edge of the cusp (Figure 4), indicating that CtCBP-1 may be involved in regulating the crystal morphology during the formation of goethite *in vivo*. In contrast, in the absence of CtCBP-1, the morphology of goethite synthesized *in vitro* was similar to that of needle-like crystals at the trailing edge of the cusp (Figure 4), except that it was less oriented. This may be due to the *in vivo* chitin fibers assisting in the orientation of the crystals.

By XRD, it is also shown that in the presence of 140 μg/mL CtCBP-1, the crystals become amorphous to a large extent as the peak at 25 degree is not sharp (Figure 5D). While the other samples and control groups (Figure 5A) showed goethite crystal type (Figures 5B, C–G). This indicates that a high concentration of CtCBP-1 can also affect the crystallization of goethite by

forming amorphous particles. The inconsistency between Raman and XRD may be due to the fact that Raman spectroscopy is a local detection method with a detection range of only a few microns and its small laser penetration depth (~5.0 μm), which is not representative of the overall structure. However, another analysis, such as TEM, is needed to clarify the results.

Binding of CtCBP-1 protein in the limpet teeth *ex vivo*

The previous study found that CtCBP-1 protein affected the morphology of needle goethite formation and that there is a concentration effect on this effect. To gain more insight into how CtCBP-1 affects goethite

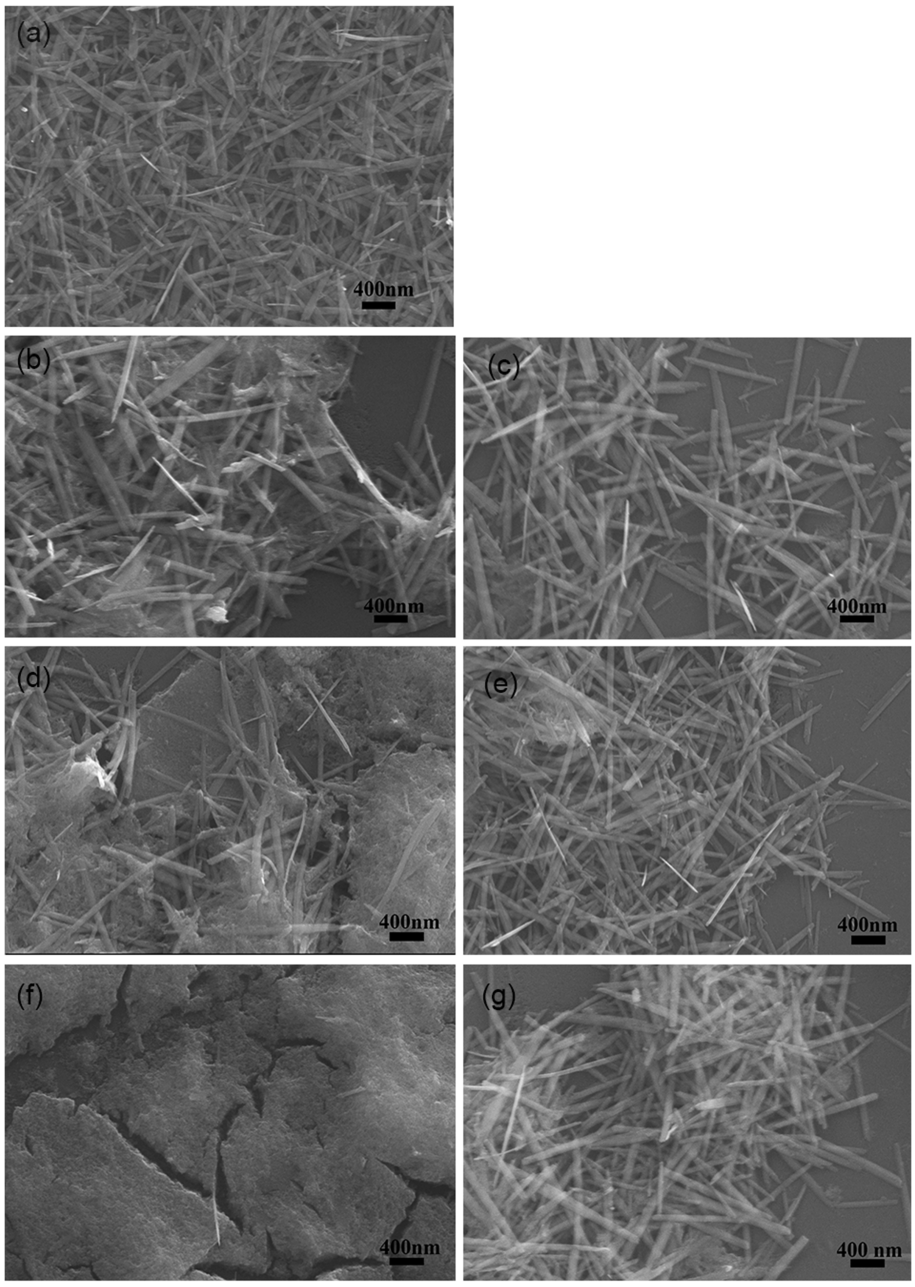

FIGURE 2
SEM images of *in vitro* goethite crystallization in the presence of CtCBP-1. **(A)** blank control, **(B)** 35 μg/ml CtCBP-1, **(C)** 35 μg/ml MBP, **(D)** 70μg/ml CtCBP-1, **(E)** 70 μg/ml MBP, **(F)** 140 μg/ml CtCBP-1, **(G)** 140 μg/ml MBP.

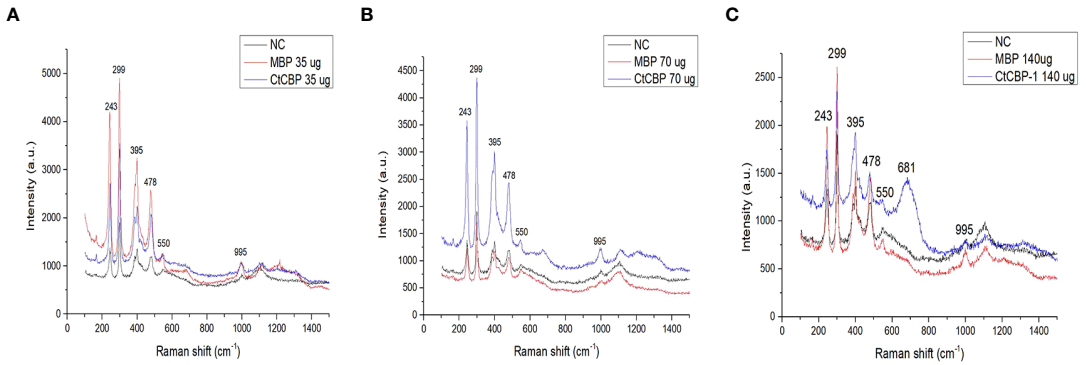

FIGURE 3
Raman spectra of the crystals with different treatment. **(A)** 35 μg/ml CtCBP-1 and 35 μg/ml MBP, **(B)** 70 μg/ml CtCBP-1 and 70 μg/ml MBP, **(C)** 140 μg/ml CtCBP-1 and 140 μg/ml MBP. NC, negative control.

crystallization, we labeled CtCBP-1 with the fluorescent dye Cy5-NHS ester and examined the localization of CtCBP-1 on the cusp. Super-resolution images were harvested at a Z-axis resolution of 0.1 μm and reconstructed as three-dimensional images by Nikon structural illumination microscopy (NSIM) at an excitation wavelength of 645 nm (Figure 6). It can be noted that the fluorescence signal shows a non-uniform distribution from the anterior to the posterior part of the cusp (Figures 6A, B). The CtCBP-1 protein labelled with Cy5 was found to bind specifically to the anterior margin of the cusp, concentrating primarily on the marginal side, whereas the MBP protein from the control (Figures 6C, D), which was uniformly distributed across the cusp, has no

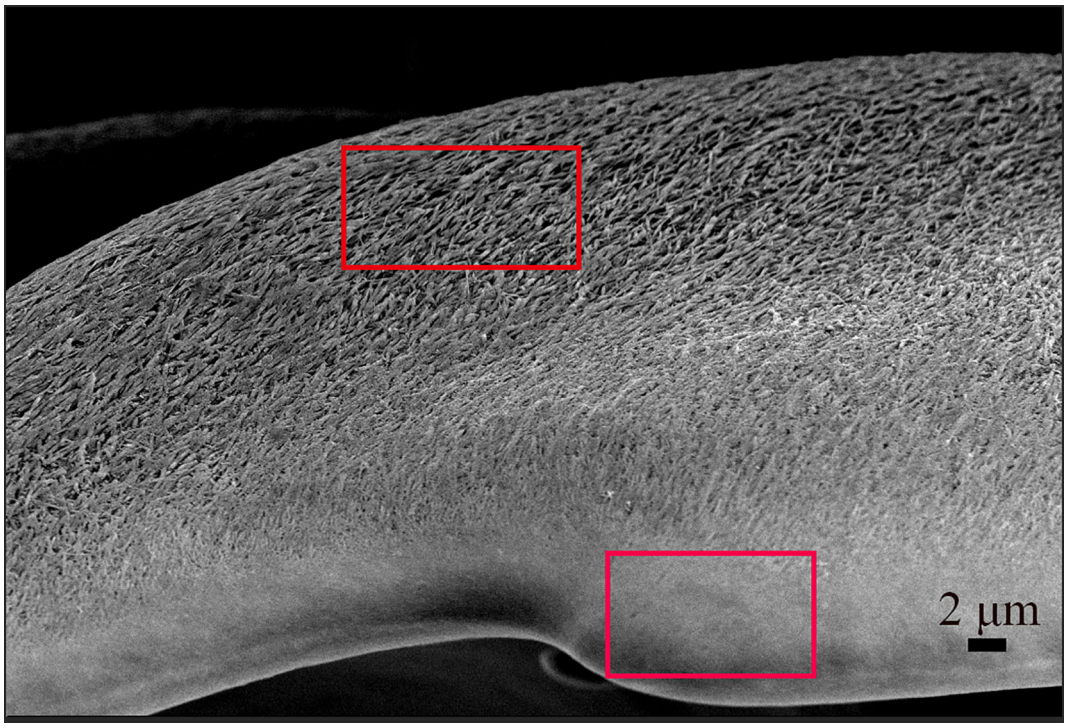

FIGURE 4
The microstructure of the limpet teeth. Bottom frame: small needles goethite packed tightly on the anterior side of the cusp; Top frame: big needles goethite packed loosely on the posterior part of the cusp.

spatial specificity. In the mollusk chiton *Acanthopleura hirtosa*, which also has a radulae structure, the anterior and posterior portions of its teeth have different densities and arrangements of chitin fibers. The chitin fibers in the anterior part of its tooth cusps gradually become sparse and lack order. In contrast, the posterior part of the tooth cusps become more organized (K. et al., 1989). We speculate that this binding result of CtCBP-1 protein is due to the fact that it contains chitin-binding sites, resulting in a higher distribution of CtCBP-1 protein in the anterior edge of the cusp where chitin fibrils are densely arranged, while chitin fibrils are sparsely arranged and have fewer protein-binding sites at the posterior edge of the cusp. Combined with previous crystallization experiments, we hypothesized that CtCBP-1, which is specifically bound at the anterior margin of the cusp, could help goethite needles to align more closely at this site or bind to the chitin fiber frame as a specific nucleation site.

Discussion

Based on the examination of the available mass spectrometry and transcriptome data, we screened the protein CtCBP-1 that has a chitin-binding domain for a more thorough investigation. We used RACE PCR to amplify a full-length fragment based on partial DNA information of CtCBP-1 in the transcriptome. Bioinformatics analysis revealed a 15 aa long signal peptide in the CtCBP-1 protein sequence, which is a secreted protein. CtCBP-1 also has a 50 aa long NG tandem repeat at the C-terminus, which is similar to those found in calcium mineralization-regulating matrix proteins reported in the literature (Miyamoto et al., 1996; Liu et al., 2015). All of these repeats have regulatory effects on crystal nucleation growth. *In vitro* binding experiments confirmed CtCBP-1's ability to bind to α-chitin and goethite. Additionally, studies on *in vitro* crystallization supported CtCBP-1's role in controlling crystalline shape. It was discovered that as the concentration of CtCBP-1 increased during crystallization, the protein altered

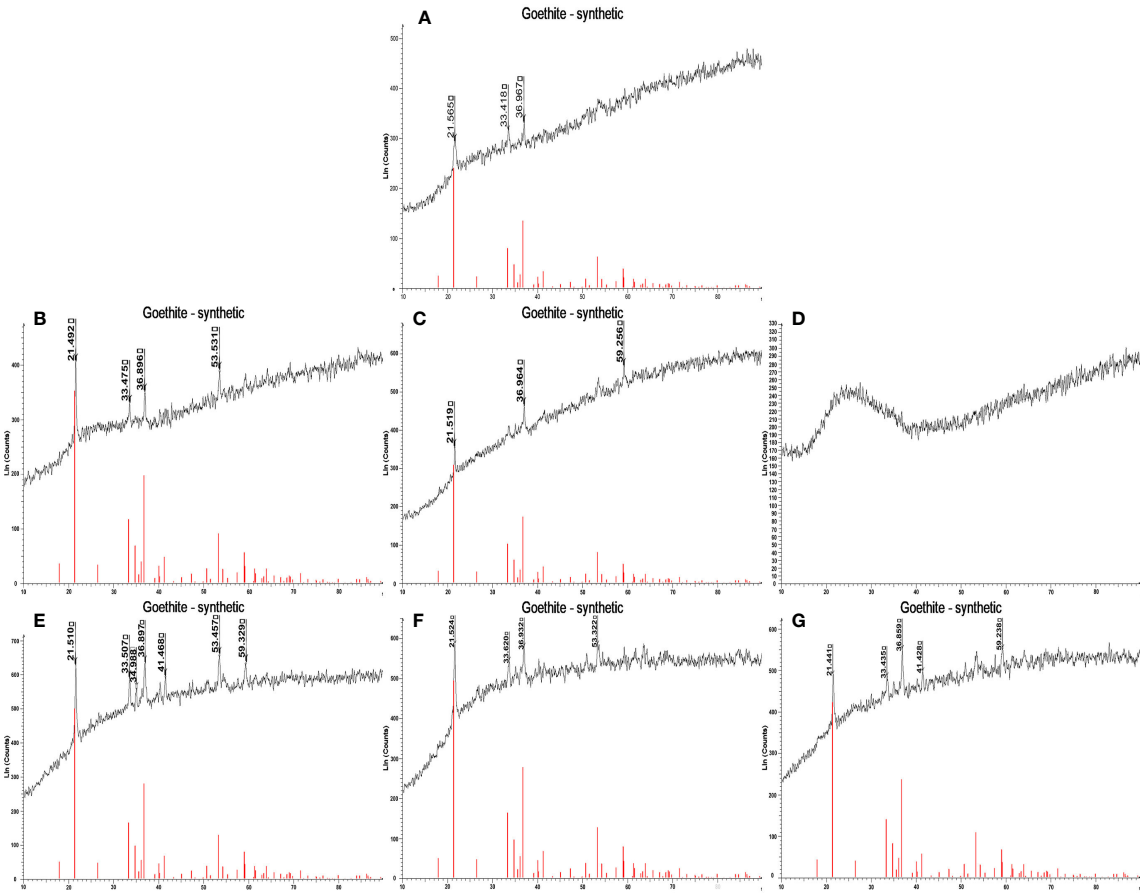

FIGURE 5
X-ray diffraction (XRD) spectra of the crystals with different treatment. **(A)** blank control, **(B)** 35 μg/ml CtCBP-1, **(C)** 70μg/ml CtCBP-1, **(D)** 140 μg/ml CtCBP-1, **(E)** 35 μg/ml MBP, **(F)** 70 μg/ml MBP, **(G)** 140 μg/ml MBP.

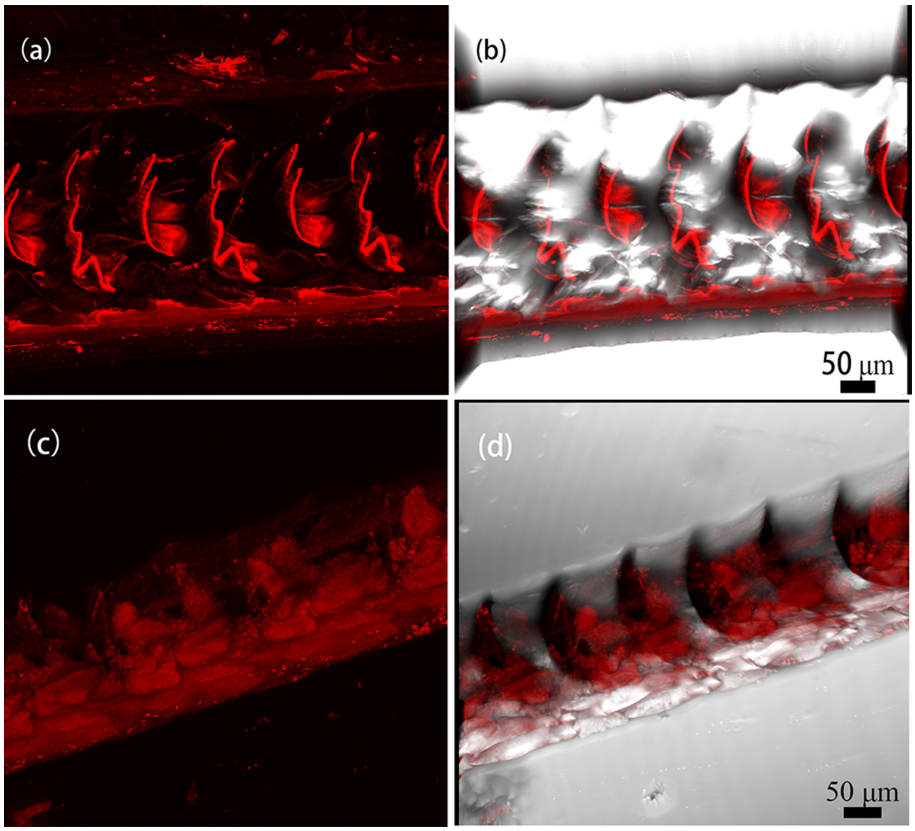

FIGURE 6
Binding of CtCBP-1-cy5 in the radulae of limpets. **(A)** binding of CtCBP-1 on radulae, **(B)** CtCBP-1, a merged image, **(C)** binding of MBP on radulae, **(D)** MBP, a merged image.

the goethite crystal morphology from needle-like to densely stacked granular. Raman spectroscopy revealed that the crystal polymorphs of α-FeOOH remained unchanged, but the XRD results revealed that the crystal changed to amorphous goethite. Finally, we examined the binding of CtCBP-1 on the radulae by Cy5 labeling and found that the CtCBP-1 specifically bound to the anterior side and edge of the cusp in the experimental group relative to the control group. When combined with the high-resolution SEM results of the cusp (Figure 4), we discovered that the crystal morphology of the anterior side of the cusps was similar to that of the high-concentration CtCBP-1 group in the *in vitro* crystallization experiments. The crystal morphology of the posterior side of the cusp was similar to that of the low-concentration CtCBP-1 test group. Therefore, we speculate that CtCBP-1 regulates the crystal morphology and crystal arrangement during the formation of goethite. The reason for this may be that the distribution of CtCBP-1 on the cusp is not uniform; it is more concentrated in the anterior region, and the high density of CtCBP-1 regulates the morphology of goethite, causing goethite crystals to change from needle-like to densely stacked granular, which is consistent with the SEM results of the cusp. The uneven binding of CtBP1 on the cusp may be related to the differential arrangement of the chitin framework, which also explains the different goethite crystal morphologies on the cusp observed by SEM.

Previous studies have shown that organic substrates, including proteins and/or polysaccharides, play a crucial role in the biomineralization of many different biominerals, such as controlling crystal nucleation and guiding the growth of crystal morphology or shape (Baeuerlein, 2006). Therefore, the study of biocrystal growth may provide new insights to improve the design and control of synthetic crystal growth. The composition and structure of limpet tooth material have been studied for over a century (SOLLAS, 1907; Lowenstam, 1962; Wal, 1989). The production process of limpet teeth, which is crucial for the development of biomimetics, has only recently been deciphered using molecular techniques. Most of the current studies on the molecular mechanisms of iron mineralization are systematic studies on the genes and proteins of the limpet tooth mineralization process using proteomic or transcriptomic approaches (Nemoto et al., 2012; Wang et al., 2018; Nemoto et al., 2019; Rumney et al., 2022). But the key matrix proteins

involved in the process of iron mineralization have not been studied in depth. No species-specific regulatory proteins associated with iron mineralization have been identified either. Studies targeting macromolecules in the mineralization of limpet or chiton teeth have focused on a few known proteins, such as ferritin. It is found that a 26 kDa ferritin subunit in the teeth of *Cellana toreuma* is translocated across the cell membrane into the teeth, resulting in the accumulation of iron in the extracellular tooth chamber and the formation of goethite needles (Lu et al., 1995). Studies on specific proteins that regulate iron oxide biomineralization are still lacking and the understanding of iron mineralization mechanisms remains incomplete.In this work, we have mined for species-specific proteins that have the ability to regulate mineralization on the basis of the transcriptome and have studied them in depth. For the first time, we report a novel chitin-binding protein who shows very high transcript level expression in the transcriptome (Wang et al., 2018). We further investigated its function and found its influence on crystal morphology during goethite synthesis. We understand that the mechanical properties of limpet tooth originate from a unique, highly organised composite structure consisting of flexible chitin nanofibers interspaced with reinforcing filamentous crystals of iron oxide in the form of goethite (α-FeO(OH)) (Runham, 1961; Lowenstam, 1962; Wal, 1989). This study contributes to our understanding of the role of macromolecular regulation of goethite in synthesis, alignment and crystal morphology.

Several issues remain to be discussed. We found that CtCBP-1 can affect the crystal morphology of goethite with a concentration gradient effect based on the results of *in vitro* crystallization experiments. Based on this finding, we explain why the goethite arrangement and crystal size difference between the anterior and posterior regions of the cusp. The regulation of goethite crystals by CtCBP-1 may be more related to the amino acid composition of the protein. According to previous studies, acidic proteins tend to appear as nucleation sites of crystals, and tandem repeats are also a common structural feature of mineralized proteins, like non-collagenous proteins in bone (George and Veis, 2008) and Asp-rich proteins in the bivalve prismatic layers (Gotliv et al., 2010). Though these proteins may be inherently unordered, their charges predict that they will interact with minerals. They are considered to perform important functions in controlling crystal polymorphism and orientation. Whether the specific role of CtCBP-1 is nucleation sites or regulation of the crystal growth process, or regulation of crystal arrangement is unclear and needs further study. In the *in vitro* crystallization experiments, the synthesized crystals are still goethite, although the crystal morphology is changed. We can further investigate whether the properties of goethite change after the addition of CtCBP-1. For example, whether the hardness of goethite is different from that of natural cusp and synthetic inorganic materials or whether the elastic modulus of goethite is optimized compared with inorganic materials. This may provide some guidance for the development of bionic research. If we can synthesize the same hardness but with altered morphology *in vitro*, this will be very important for the next step of bionanotechnology research.

Data availability statement

The datasets presented in this study can be found in online repositories. The names of the repository/repositories and accession number(s) can be found in the article/ Supplementary Material.

Author contributions

Conceptualization, YW. Methodology, YW. Validation, YW. Writing-original draft preparation, YW. Writing—review and editing, CL. Project administration, RZ. Funding acquisition, YW. All authors contributed to the article and approved the submitted version.

Funding

This study was supported by Fundamental Research Funding of Beijing Technology and Business University (PXM2020_014213_000017)

Acknowledgments

We thank Dr. Dong Yang for helpful discussion on this paper.

Conflict of interest

The authors declare that the research was conducted in the absence of any commercial or financial relationships that could be construed as a potential conflict of interest.

Publisher's note

References

Amemiya, Y., Arakaki, A., Staniland, S. S., Tanaka, T., and Matsunaga, T. (2007). Controlled formation of magnetite crystal by partial oxidation of ferrous hydroxide in the presence of recombinant magnetotactic bacterial protein Mms6. *Biomaterials.* 28 (35), 5381–5389. doi: 10.1016/j.biomaterials.2007.07.051

Athanasiadou, D., Jiang, W., Goldbaum, D., Saleem, A., Basu, K., Pacella, M. S., et al. (2018). Nanostructure, osteopontin, and mechanical properties of calcitic avian eggshell. *Sci Adv*) 4 (1200 New York Ave NW, Washington, DC 20005: Amer Assoc Advancement Science). doi: 10.1126/sciadv.aar3219

Baeuerlein, E. (2006). *Biomineralization: Progress in biology, molecular biology and application, 2nd, completely revised and extended edition*. (Weinheim: WILEY-VCH)

Barber, A. H., Lu, D., and Pugno, N. M. (2015). Extreme strength observed in limpet teeth. *J. R Soc. Interface.* 12 (105). doi: 10.1098/rsif.2014.1326

Brooker, L. R., and Shaw, J. A. (2012). *The chiton radula: A unique model for biomineralization studies. Advanced Topics in Biomineralization* 1, 65–84.

Burford, M. A., Macey, D. J., and Webb, J. (1986). Hemolymph ferritin and radula structure in the limpets patelloida alticostata and patella peronii (Mollusca: Gastropoda). *Comp. Biochem. Physiol. – Part A: Physiol.* 83 (2), 353–358. doi: 10.1016/0300-9629(86)90589-X

Cornell, R. M., and Schneider, W. (1989). Formation of goethite from ferrihydrite at physiological pH under the influence of cysteine. *Polyhedron.* 8 (2), 149–155. doi: 10.1016/S0277-5387(00)86496-7

Faivre, D., and Godec, T. U. (2015). From bacteria to mollusks: the principles underlying the biomineralization of iron oxide materials. *Angewandte Chemie Int. Edition.* 54 (16), 4728–4747. doi: 10.1002/anie.201408900

Fang, D., Pan, C., Lin, H., Lin, Y., Zhang, G., Wang, H., et al. (2012). Novel basic protein, PfN23, functions as key macromolecule during nacre formation. *J. Biol. Chem.* 287 (19), 15776–15785. doi: 10.1074/jbc.M112.341594

George, A., and Veis, A. (2008). Phosphorylated proteins and control over apatite nucleation, crystal growth, and inhibition. *Chem. Rev.* 108 (11), 4670–4693. doi: 10.1021/cr0782729

Gotliv, B. A., Kessler, N., Sumerel, J. L., Morse, D. E., Tuross, N., Addadi, L., et al. (2010). Asprich: A novel aspartic acid-rich protein family from the prismatic shell matrix of the bivalve atrina rigida. *Chembiochem.* 6 (2), 304–314. doi: 10.1002/cbic.200400221

Grime, G. W., Watt, F., Mann, S., Perry, C. C., Webb, J., and Williams, R. J. P. (1985). Biological applications of the Oxford scanning proton microprobe. *Trends Biochem. Sci.* 10 (1), 6–10. doi: 10.1016/0968-0004(85)90005-2

Grunenfelder, L. K., de Obaldia, E. E., Wang, Q. Q., Li, D. S., Weden, B., Salinas, C., et al. (2014). Stress and damage mitigation from oriented nanostructures within the radular teeth of cryptochiton stelleri. *Adv. Funct. Mater.* 24 (39), 6093–6104. doi: 10.1002/adfm.201401091

Hilgers, L., Hartmann, S., Hofreiter, M., and von Rintelen, T. (2018). Novel genes, ancient genes, and gene co-option contributed to the genetic basis of the radula, a molluscan innovation. *Mol. Biol. evolution.* 35 (7), 1638–1652. doi: 10.1093/molbev/msy052

Kim, K.-S., Macey, D. J., Webb, J., and Mann, S. (1989). Iron mineralization in the radula teeth of the chiton acanthopleura hirtosa. *Proc. R. Soc. B Biol. Sci.* 237, 335–346. doi: 10.1098/rspb.1989.0052

Liddiard, K. J., Hockridge, J. G., Macey, D. J., Webb, J., and Bronswijk, W. V. (2004). Mineralisation in the teeth of the limpets patelloida alticostata and scutellastra laticostata (Mollusca: Patellogastropoda). *Molluscan Res.* 24 (1), 21–31. doi: 10.1071/MR03012

Lin, S., Li, M., Dujardin, E., Girard, C., and Mann, S. (2005). One-dimensional plasmon coupling by facile self-assembly of gold nanoparticles into branched chain networks. *Advanced Materials.* 17 (21), 2553–2559. doi: 10.1002/adma.200500828

Liu, C., Li, S., Huang, J., Liu, Y., Jia, G., Xie, L., et al. (2015). Extensible byssus of pinctada fucata: Ca2+-stabilized nanocavities and a thrombospondin-1 protein. *Rep.* 5, 15018. doi: 10.1038/srep15018

Lowenstam, H. A. (1962). Goethite in radular teeth of recent marine gastropods. *Science.* 137, 279–2 80. doi: 10.1126/science.137.3526.279

Lowenstam, H. A. (1981). Minerals formed by organisms. *Science.* 211 (4487), 1126–1131. doi: 10.1126/science.7008198

Lowenstam, H. A., and Weiner, S. (1989). *On biomineralization: Oxford university press on demand.* (New York: Oxford University Press)

Lu, H. K., Huang, C. M., and Li, C. W. (1995). Translocation of ferritin and biomineralization of goethite in the radula of the limpet cellana toreuma reeve. *Exp. Cell Res.* 219 (1), 137–145. doi: 10.1006/excr.1995.1214

Mann, S., Perry, C. C., Webb, J., Luke, B., and Williams, R. J. P. (1986). Structure, morphology, composition and organization of biogenic minerals in limpet teeth. *Proc. R. Soc. London* 227 (1247), 179–190. doi: 10.1098/rspb.1986.0018

Marie, P., Labas, V., Brionne, A., Harichaux, G., Hennequet-Antier, C., Nys, Y., et al. (2015). Quantitative proteomics and bioinformatic analysis provide new insight into protein function during avian eggshell biomineralization. *J. Proteomics.* 113, 178–193. doi: 10.1016/j.jprot.2014.09.024

Martins, E., Rocha, M. S., Silva, T. H., and Reis, R. L. (2019). "Remarkable body architecture of marine sponges as biomimetic structure for application in tissue engineering," in *Marine-derived biomaterials for tissue engineering applications*. Eds. A. H. Choi and B. Ben-Nissan (Singapore: Springer Singapore), 27–50.

Miyamoto, H., Miyashita, T., and Okushima, M. (1996). A carbonic anhydrase from the nacreous layer in oyster pearl. *Proc. Natl. Acad. Sci. United States America* 93 (18), 9657–9660. doi: 10.1073/pnas.93.18.9657

Mohapatra, M., Sahoo, S. K., Mohanty, C. K., Das, R. P., and Anand, S. (2005). Effect of Ce(IV) doping on formation of goethite and its transformation to hematite. *Materials Chem. Phys.* 94 (2/3), 417–422. doi: 10.1016/j.matchemphys.2005.05.024

Nemoto, M., Ren, D., Herrera, S., Pan, S., Tamura, T., Inagaki, K., et al. (2019). Integrated transcriptomic and proteomic analyses of a molecular mechanism of radular teeth biomineralization in cryptochiton stelleri. *Sci. Rep.* 9, 856. doi: 10.1038/s41598-018-37839-2

Nemoto, M., Wang, Q., Li, D., Pan, S., Matsunaga, T., and Kisailus, D. (2012). Proteomic analysis from the mineralized radular teeth of the giant pacific chiton, cryptochiton stelleri (Mollusca). *Proteomics.* 12 (18), 2890–2894. doi: 10.1002/pmic.201100473

Nielsen, H. (2017). "Predicting secretory proteins with SignalP," in *Protein function prediction: Methods and protocols*. Ed. D. Kihara (New York, NY: Springer New York), 59–73.

Pierre, T. G. S., Mann, S., Webb, J., Dickson, D. P. E., Runham, N. W., and Williams, R. J. P. (1986). Iron oxide biomineralization in the radula teeth of the limpet patella vulgata; mossbauer spectroscopy and high resolution transmission electron microscopy studies. *Proc. R. Soc. London* B228 (1250), 31–42. doi: 10.1098/rspb.1986.0038

Ramos-Silva, P., Kaandorp, J., Huisman, L., Marie, B., Zanella-Cleon, I., Guichard, N., et al. (2013). The skeletal proteome of the coral acropora millepora: the evolution of calcification by co-option and domain shuffling. *Mol. Biol. Evol.* 30 (9), 2099–2112. doi: 10.1093/molbev/mst109

Ruggeberg, M., Burgert, I., and Speck, T. (2010). Structural and mechanical design of tissue interfaces in the giant reed arundo donax. *J. R Soc. Interface.* 7 (44), 499–506. doi: 10.1098/rsif.2009.0273

Rumney, R. M., Robson, S. C., Kao, A. P., Barbu, E., Bozycki, L., Smith, J. R., et al. (2022). Biomimetic generation of the strongest known biomaterial found in limpet tooth. *Nat. Commun.* 13 (1), 1–13. doi: 10.1038/s41467-022-31139-0

Runham, N. W. (1961). The histochemistry of the radula of patella vulgata. *J. Cell Sci.* s3-102, 371–380. doi: 10.1242/jcs.s3-102.59.371

SOLLAS, I. B. J. (1907). Memoirs: The molluscan radula: its chemical composition, and some points in its development. *J. Cell Sci.* s2-51 (201), 115–136. doi: 10.1242/jcs.s2-51.201.115

Sone, E. D., Weiner, S., and Addadi, L. (2005). Morphology of goethite crystals in developing limpet teeth: Assessing biological control over mineral formation. *Cryst Growth Des.* 5 (6), 2131–2138. doi: 10.1021/cg050171l

Sone, E. D., Weiner, S., and Addadi, L. (2007). Biomineralization of limpet teeth: a cryo-TEM study of the organic matrix and the onset of mineral deposition. *J. Struct. Biol.* 158 (3), 428–444. doi: 10.1016/j.jsb.2007.01.001

Stegbauer, L., Smeets, P. J., Free, R., Wallace, S. G., Hersam, M. C., Alp, E. E., et al. (2021). Persistent polyamorphism in the chiton tooth: From a new biomineral to inks for additive manufacturing. *Proc. Natl. Acad. Sci.* 118 (23), e2020160118. doi: 10.1073/pnas.2020160118

Tanaka, M., Mazuyama, E., Arakaki, A., and Matsunaga, T. (2011). MMS6 protein regulates crystal morphology during nano-sized magnetite biomineralization in vivo. *J. Biol. Chem.* 286 (8), 6386–6392. doi: 10.1074/jbc.M110.183434

Ukmar-Godec, T., Kapun, G., Zaslansky, P., and Faivre, D. (2015). The giant keyhole limpet radular teeth: A naturally-grown harvest machine. *Academic Press Inc Elsevier Science* 192, 92101–4495. doi: 10.1016/j.jsb.2015.09.021

van der Wal, P., Giesen, H. J., and Videler, J. J. (2000). Radular teeth as models for the improvement of industrial cutting devices. *Mat Sci. Eng. C-Bio S.* 7 (2), 129–142. doi: 10.1016/S0928-4931(99)00129-0

Wal, P. V. D. (1989). Structural and material design of mature mineralized radula teeth of patella vulgata (gastropoda). *J. Ultrastructure Res. Mol. Structure Res.* 102 (2), 147–161. doi: 10.1016/0889-1605(89)90052-9

Wang, Y. D., Liu, C., Du, J. Z., Huang, J. L., Zhang, S. C., and Zhang, R. Q. (2018). The microstructure, proteomics and crystallization of the limpet teeth. *Proteomics* 18 (19), 1800194. doi: 10.1002/pmic.201800194

Weaver, J. C., Wang, Q. Q., Miserez, A., Tantuccio, A., Stromberg, R., Bozhilov, K. N., et al. (2010). Analysis of an ultra hard magnetic biomineral in chiton radular teeth. *Mater Today* 13 (1-2), 42–52. doi: 10.1016/S1369-7021(10)70016-X

Weiner, S., and Dove, P. M. (2003). An overview of biomineralization processes and the problem of the vital effect. *Rev. mineralogy geochemistry.* 54 (1), 1–29. doi: 10.2113/0540001

YerPeng,, Tan,, Shawn,, Hoon,, Paul,, Guerette,, et al. (2015). Infiltration of chitin by protein coacervates defines the squid beak mechanical gradient. *Nat. Chem. Biol.* 11, 488–495. doi: 10.1038/nchembio.1833